Geophysical Journal International

*Geophys. J. Int.* (2018) **214,** 1623–1632
Advance Access publication 2018 June 04
GJI Gravity, geodesy and tides

doi: 10.1093/gji/ggy220

# Gravity interpretation to image the geologic structures of the coastal zone in al Qunfudhah area, southwest Saudi Arabia

Aseem Sulaiman,[1] Eslam Elawadi[2,3] and Saad Mogren[2]

[1] *King Abdulaziz City for Science and Technology, Riyadh 12371,Kingdom of Saudi Arabia*
[2] *King Saud University, Riyadh 11451, Kingdom of Saudi Arabia. E-mail: e_elawadi@yahoo.com*
[3] *Nuclear Materials Authority of Egypt, Egypt.*

Accepted 2018 June 2. Received 2018 May 28; in original form 2017 December 25

## SUMMARY

This study provides interpretation and modelling of gravity survey data to map the subsurface basement relief and controlling structures of a coastal area in the southwestern part of Saudi Arabia as an aid to groundwater potential assessment. The gravity survey data were filtered and analysed using different edge detection and depth estimation techniques and concluded by 2-D modelling conducted along representative profiles to obtain the topography and depth variations of the basement surface in the area. The basement rocks are exposed in the eastern part of the area but dip westward beneath a sedimentary cover to depths of up to 2200 m in the west, while showing repeated topographic expressions related to a tilted fault-block structure that is dominant in the Red Sea rift zone. Two fault systems were recognized in the area. The first is a normal fault system trending in the NNW–SSE direction that is related to the Red Sea rift, and the second is a cross-cutting oblique fault system trending in the NE–SW direction. The interaction between these two fault systems resulted in the formation of a set of closed basins elongated in the NNW–SSE direction and terminated by the NE–SW fault system. The geomorphology and sedimentary sequences of these basins qualify them as potential regions of groundwater accumulation.

**Key words:** Structure of the Earth; Gravity anomalies and Earth structure; Numerical modelling.

## 1 INTRODUCTION

The study area is located at the eastern coast of the Red Sea, southwest Saudi Arabia (Fig. 1). The area includes many of the relatively large cities along the major wadis to the southwest of escarpments such as the Muzailaf, Helli, Dukeh, Al Quoz and Bani Zeid, and has a population of about 900 000 people. These people depend on desalination of seawater and treatment of rainwater accumulated by dams for their drinking water. However, agricultural and tourist developments in this area have increased the demand for both drinking water and irrigation water, and groundwater is considered to be one of the most suitable sources to meet this water demand. Therefore, a study of the groundwater potential of the area is an important task to guide drilling programs to the most promising areas for groundwater accumulations.

The study area is a part of Asir mountainous chain, running parallel to the Red Sea in southwestern Saudi Arabia. Asir mountainous region has the highest average rainfall of Saudi Arabia (from 500 to 1000 mm $yr^{-1}$) largely due to seasonal rain. These mountains form steep escarpments that drop westwards to the Tihamah plain on the Red Sea coast. Therefore, most of the rainwater run to the west through short wadis, drain to the Red Sea, if not trapped by dams or penetrates to the subsurface aquifers as groundwater.

This work aims to contribute to the evaluation of the groundwater potential of the area through interpretation of the detailed gravity survey data available in order to estimate depth to the basement surface beneath the coastal sediments, map the sedimentary basins formed due to structural variation of the basement depth and relate these basins to the groundwater potential that might exist in the study area.

## 2 GENERAL GEOLOGY

The study area is part of the southwestern zone of the Arabian Shield at the eastern coast of the Red Sea (Fig. 1). The geology of the area was compiled within the Al Qunfudhah Quadrangle by Prinz (1984) from older reconnaissance 1:100 000-scale geologic maps. The eastern strip of the area consists of Arabian Shield rocks represented by metamorphosed volcanic and sedimentary rocks of the late Proterozoic age (Baish and Baha groups, 1000–800 Ma). These older rocks were folded and intruded by Proterozoic plutonic and hypabyssal intrusive tonalite and diorite batholiths (800–890 Ma).

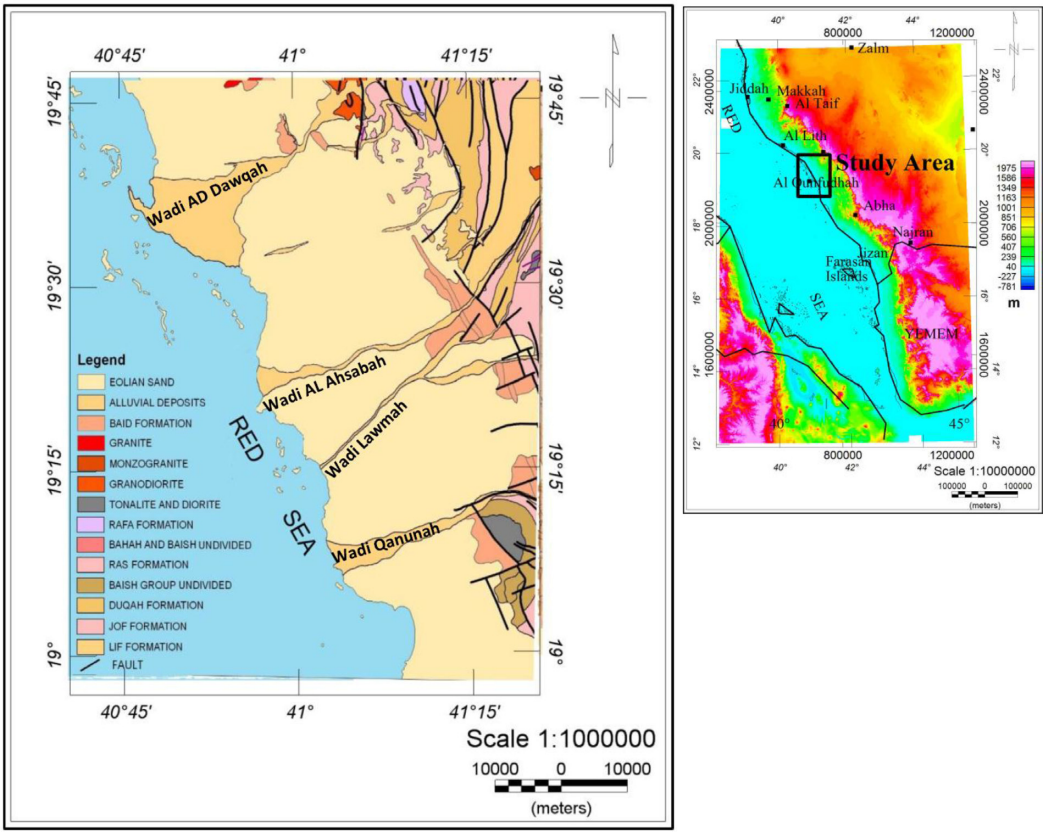


**Figure 1.** Location and geologic maps of the study area.

These events were followed by deposition of the Ablah Group, which ended at 763 Ma with the diapiric intrusion of monzogranite to granodiorite. This intrusive event was accompanied by regional metamorphism to greenschist–amphibolite facies, folding and faulting.

During the Miocene, northwest-trending faults related to rifting along the axis of the Red Sea formed, and some of these were intruded by gabbro. Basaltic lavas flowed from fissures near the Red Sea Escarpment, eastwards into low areas and westwards down several wadis below the escarpment (Prinz 1984). The aforementioned basaltic rocks in the central and western parts of the area are covered by Quaternary coastal sediments, wadi deposits and eolian sediments consisting of sand, gravel and silt.

Topographically, the eastern part of the area is dominated by the Red Sea Escarpment, which trends northwest, has a maximum altitude of about 1000 m, and declines steeply to the west. The area below and to the south of the escarpment is marked by small mountains and ridges that range in altitude from 100 to 300 m. A relatively flat coastal plain, 25 to 40 km wide, extends from the mountainous area southwest to the Red Sea. Watershed analysis of the Shuttle Radar Topography Mission (SRTM) data reveals a system of narrow elongated catchment areas with dense stream networks (Fig. 2). The rainwater flows through the drainage system from Asir mountainous ridges to the low land at the coastal plain. Most of the coastal plain consists of sedimentary layers and friable deposits overlie the complex basement dipping in general westward to the Red Sea. As a result, considerable amount of the runoff water can penetrate through these sediments, and accumulates in the basin areas of the basement surface. Tilted faulted block structure system dominated in the Red Sea rift qualifies the basement surface of the coastal areas to form basins that can be considered as suitable groundwater aquifers.

## 3 GRAVITY DATA AND ANALYSIS

### 3.1 Gravity data

The Saudi ARAMCO oil company has conducted a detailed seismic and gravity survey covering most of the southern coastal plain, including the study area. The gravity data covering the study area were collected along 53 profiles parallel and perpendicular to the Red Sea coast (Fig. 3). The gravity station separation was about 250 m in general and about 500 m in some profiles. The line spacing ranged from 1000 m in the centre of the area to 2500 m at the boundaries

The gravity data were corrected to eliminate the inherent effect of crustal thickness variation in the costal zones. Anomalies caused by isostatic compensation are most pronounced in the western part of the area due to the crustal thinning at the Red Sea rift zone. A regional isostatic gravity field was removed from the Bouguer gravity anomaly by assuming an Airy–Heiskanen model for isostatic compensation of topographic loads (Simpson *et al.* 1983). On the basis of the mantle compressional wave velocities measured for the Saudi Arabian section (Healy *et al.* 1982), this model assumed a crustal density of 2.94 g $cm^{-3}$, a normal crustal thickness at sea level of 33.7 km and a density contrast across the base of the model crust of 0.34 g $cm^{-3}$ (Gettings 1983). The resulted isostatic residual gravity anomaly map (Fig. 4) was further enhanced and analysed using the following analysis techniques.

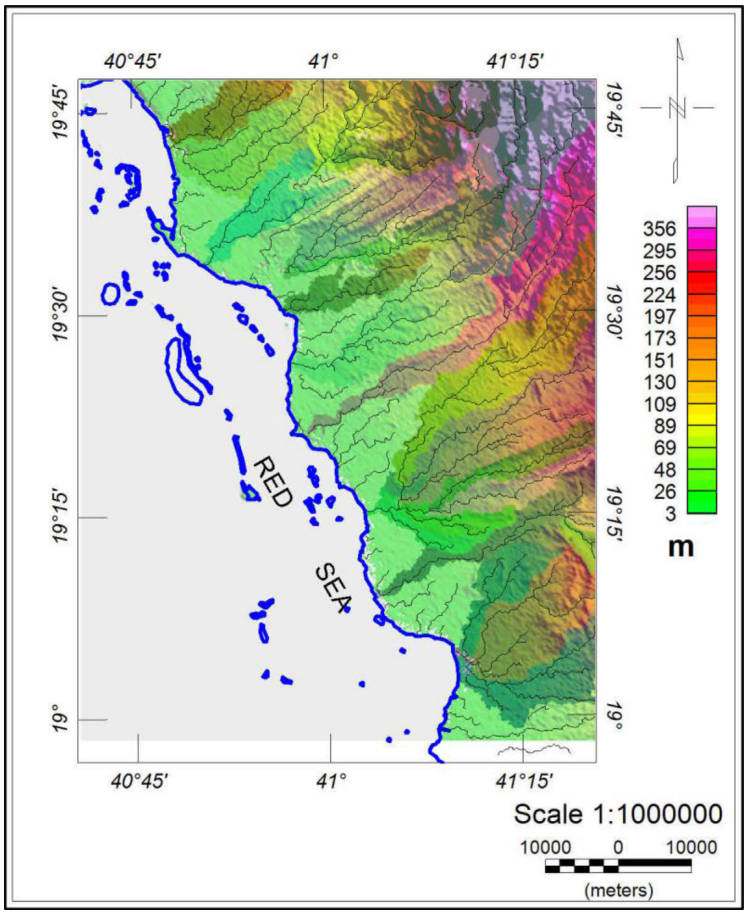


**Figure 2.** Topographic map of the study area showing the drainage pattern and watershed zones.

### 3.2 Data filtering

Subsequently, the isostatic residual gravity anomaly data were filtered, in frequency domain, to enhance the dataset and make the anomalies easier to interpret in terms of their geological sources (Bird 1997). The most effective way to filter such data is with an understanding of the geologic control and the desired filtered results. One of traditional filters, used for potential field data, is the separation of long- and short-wavelength anomalies. The success of this technique depends on the proper choice of the cut-off wavenumber applied. The cut-off wavenumbers and information about the contribution of the short and long wavenumbers in the spectrum can be obtained from the calculated radially averaged power spectrum of the data.

The 2-D power spectrum curve of the isostatic residual gravity anomaly data (Fig. 4) shows a hump phenomenon between 0 and 0.03 wavenumber $km^{-1}$. This hump shape is an indication of lower crustal sources that might be associated with deep-seated variation of density in the transition between the oceanic and continental crust. Moreover, there are two linear segments related to long- and short-wavelength components with frequency bands ranging from 0.03 to 0.1 and from 0.1 to 0.4 wavenumbers $km^{-1}$, respectively (Fig. 5). The frequency bands corresponding to these linear segments were used through the band-pass filter technique to produce the regional (Fig. 6) and residual (Fig. 7) gravity maps. These regional and residual maps were used for structural interpretation and trend analysis. Both the regional and residual gravity maps are believed to represent the basement surface and the sedimentary section. Therefore, band-pass filter technique with frequency band from 0.03 to 0.4 wavenumbers $km^{-1}$ (wavelength of about 33 to 2.5 km) was applied to the isostatic residual gravity anomaly map to filter out the effect of the very deep sources. The produced map (Fig. 8), combined the gravity signals of the regional and residual maps, was used for quantitative interpretation, such as depth estimation and modelling techniques.

### 3.3 Source edge detection

The source edge detection (SED) technique (Oasis montaj$^{TM}$) is an automatic technique that calculates the horizontal gradient of the gravity data to image the edges of the causative sources. The method searches for localized peaks in the gradient grid (Blakely & Simpson 1986), showing these points as symbols aligned parallel to the strike direction of the edges (contacts) and pointing to the 'down-gradient' direction by a dip indicator. When plotted using the regional and residual Bouguer grids, these symbols identify the deep and shallow geological contacts, respectively. This method is independent of interpreter subjective view and provides the direction of the picked contact, which can be used further for trend analysis techniques. The SED technique was applied to delineate the deep-seated and near-surface structures. The estimated strike directions of the mapped structures enabled direct analysis of structural trends. Deep-seated structures trend NNW–SSE (Red Sea trend), and shallow structures have NNW–SSE as well as minor NE–SW trends.

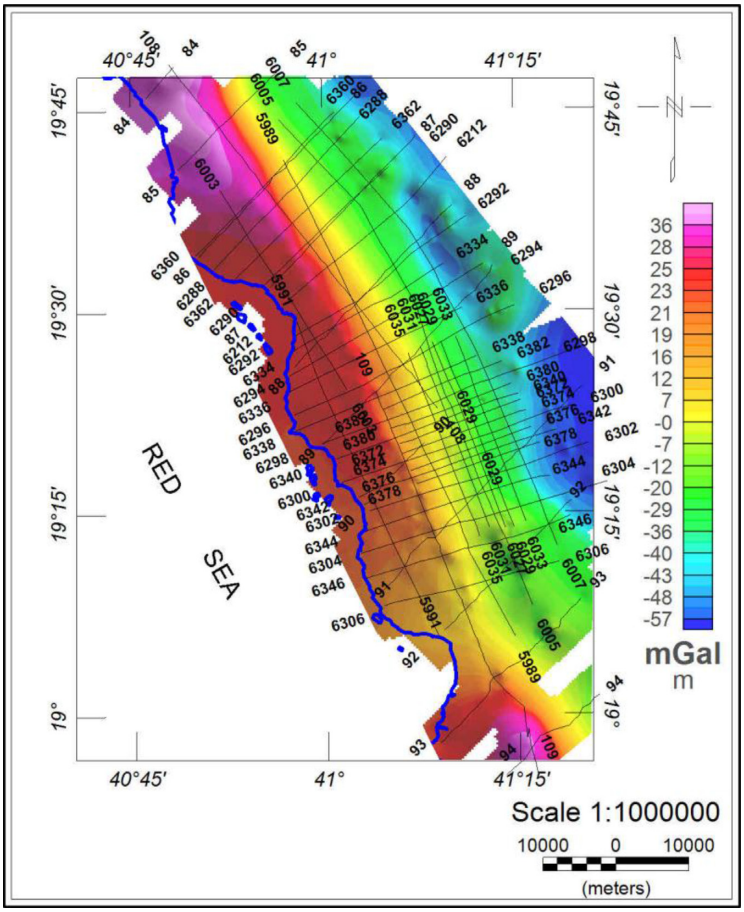


**Figure 3.** Bouguer gravity map showing the gravity survey lines.

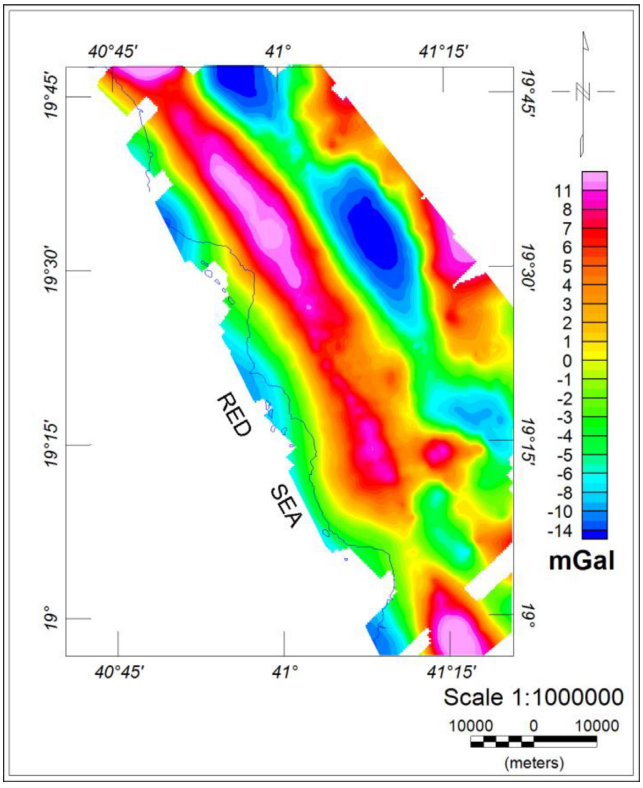


**Figure 4.** Isostatic residual gravity anomaly map.

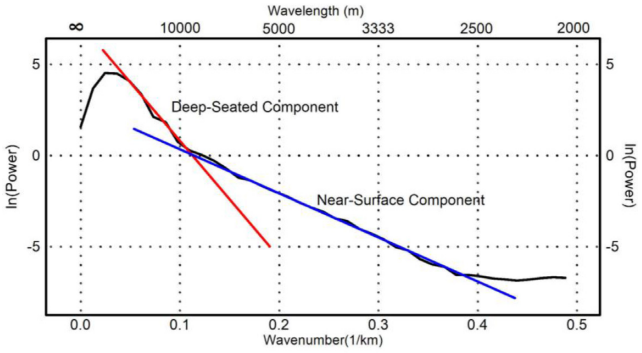


**Figure 5.** Radially averaged power spectrum of isostatic residual gravity anomaly data (Fig. 4).

### 3.4 Euler deconvolution

Euler deconvolution (ED) is an automatic interpretation technique adapted by Thompson (1982) from the homogeneity equation written by Hood (1965) to develop a procedure for interpreting 2-D gravity and magnetic anomalies. Reid *et al.* (1990) extended the Euler method for use on grid-based data. Euler's homogeneity equation can be written as (Thompson 1982)

$$(x - x_\circ)\frac{\partial g}{\partial x} + (y - y_\circ)\frac{\partial g}{\partial y} + (z - z_\circ)\frac{\partial g}{\partial z} = -Ng, \qquad (1)$$

where $\frac{\partial g}{\partial x}$, $\frac{\partial g}{\partial y}$ and $\frac{\partial g}{\partial z}$ represent the first-order derivatives of the observed anomalies along the $x$-, $y$-, and $z$-directions, respectively, and

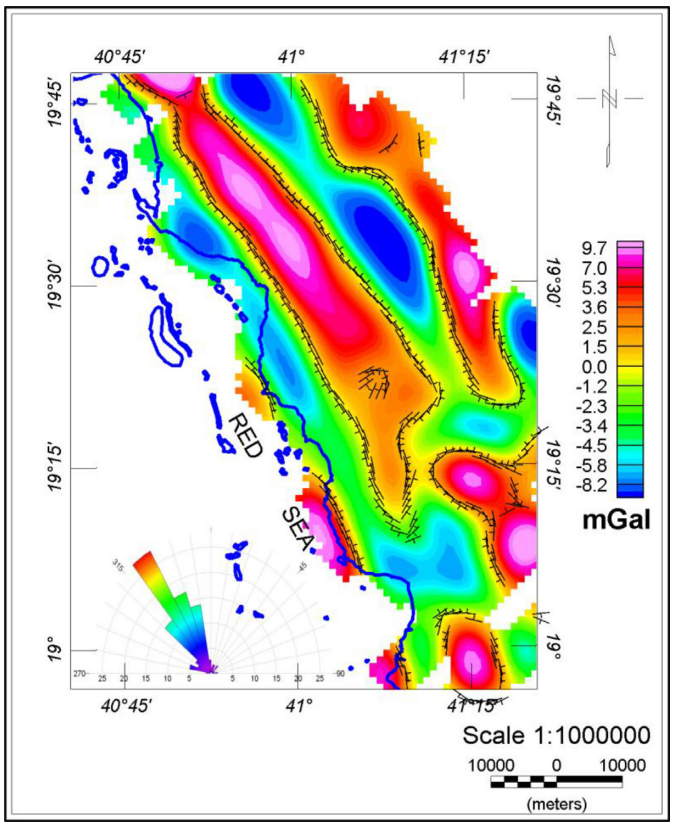


**Figure 6.** Source edge detection and trend analysis for the regional Bouguer gravity data.

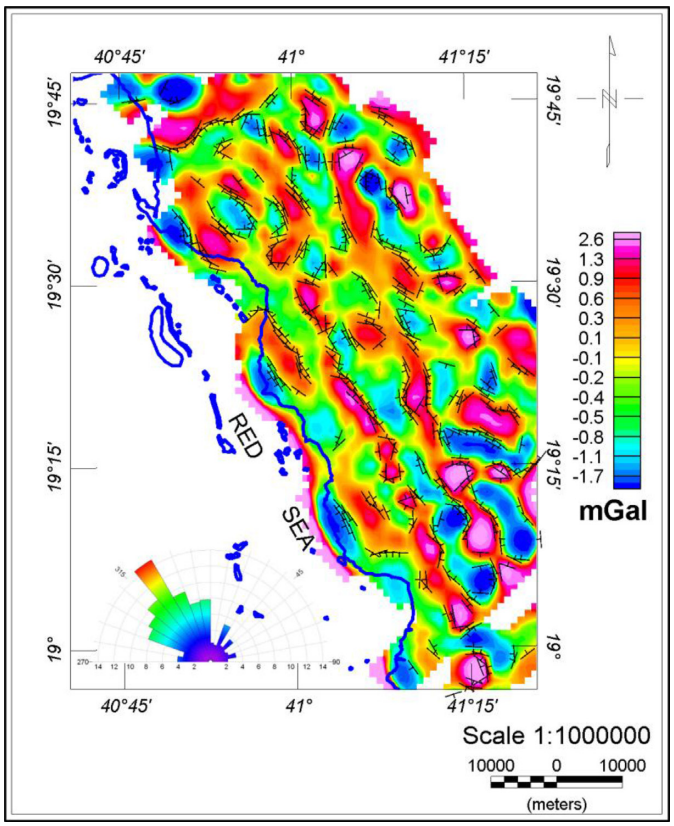


**Figure 7.** Source edge detection and trend analysis for the residual Bouguer gravity data.

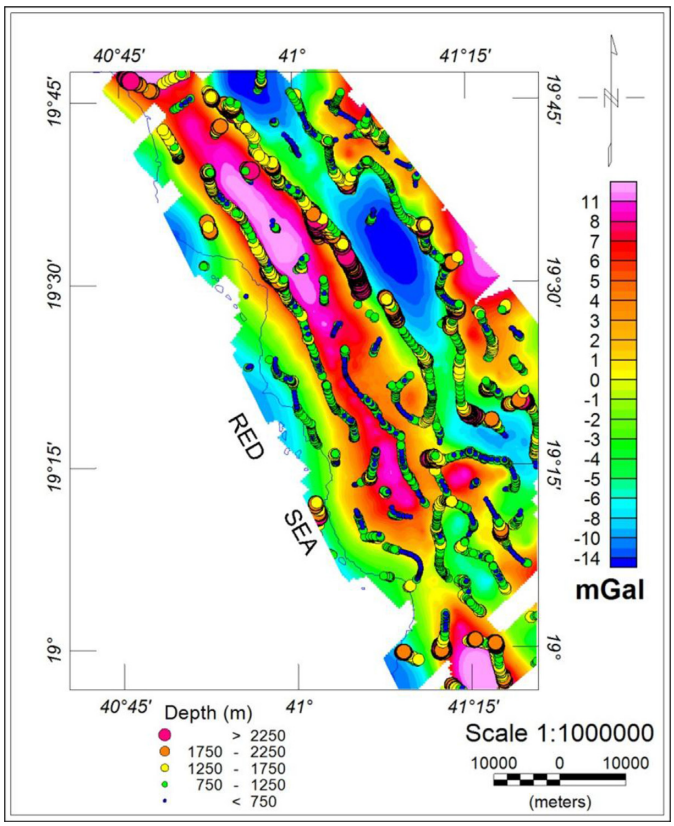


**Figure 8.** Euler deconvolution solutions for the first vertical derivative (FVD) of filtered isostatic residual gravity anomaly data, using the contact structure index of SI = 0.

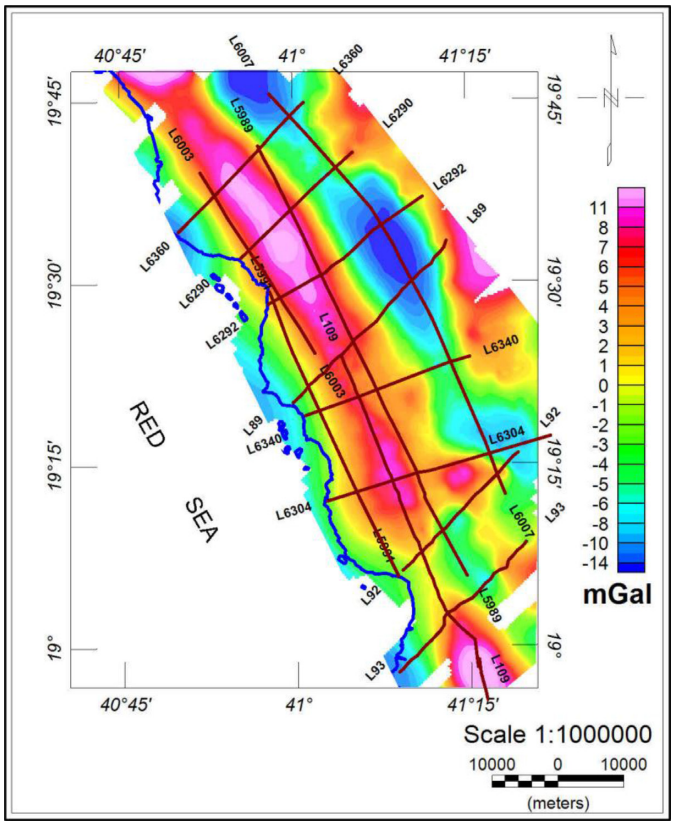


**Figure 9.** Filtered isostatic residual gravity anomaly map showing the locations of the profiles selected for 2-D modelling.

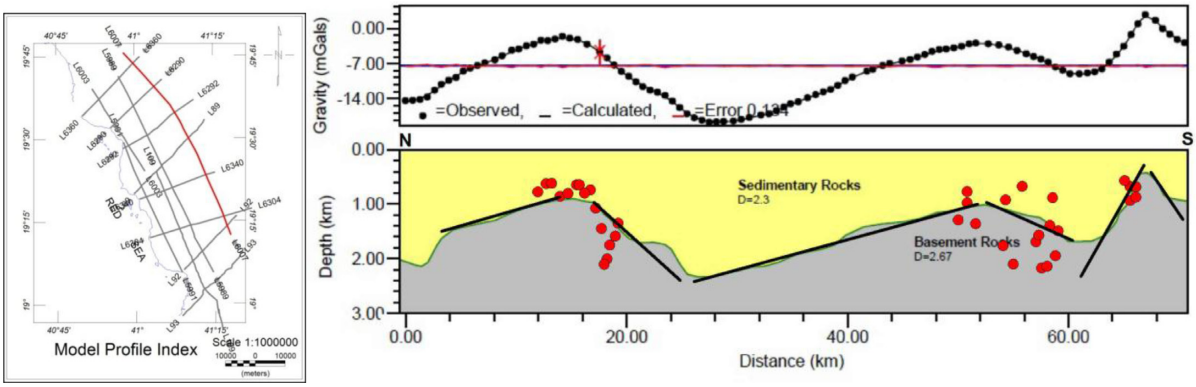


**Figure 10.** 2-D gravity model for a profile parallel to the Red Sea (Line 6007) running from north to south as shown in the inset index map. Red circles showing the Euler solutions for contact model.

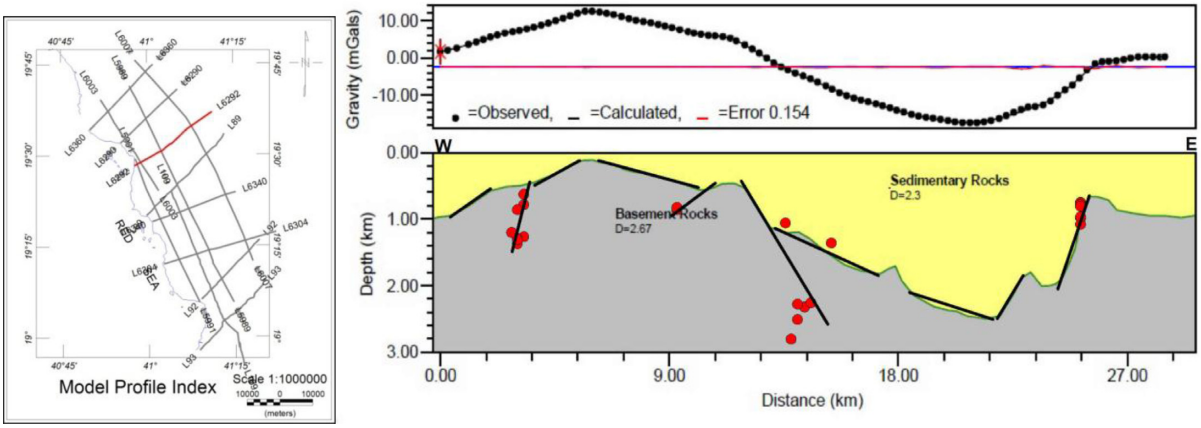


**Figure 11.** 2-D gravity model for a profile perpendicular to the Red Sea (Line 6292) running from west to east as shown in the inset index map. Red circles showing the Euler solutions for contact model.

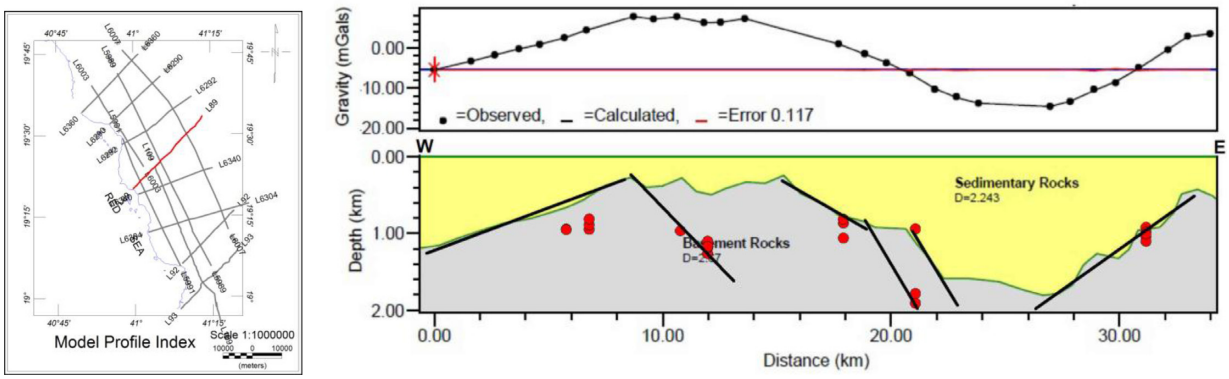


**Figure 12.** 2-D gravity model for a profile perpendicular to the Red Sea (Line 89) running from west to east as shown in the inset index map. Red circles showing the Euler solutions for contact model.

$N$ is known as a structural index related to the nature of the gravity source. For example, $N = 2$ is for a point mass, $N = 1$ corresponds to an infinite horizontal and semi-infinite vertical line of masses, $N = 1$–$2$ is associated with a finite horizontal and vertical line of masses, $N = 0$–$1$ for a 2-D vertical ribbon and $N = -1$ for a contact model (Stavrev 1997; Roy *et al.* 2000). Taking into account a base level for the regional gravity field ($B$), eq. (1) can be rearranged and written as

$$x_\circ \frac{\partial g}{\partial x} + y_\circ \frac{\partial g}{\partial y} + z_\circ \frac{\partial g}{\partial z} + NB = x\frac{\partial g}{\partial x} + y\frac{\partial g}{\partial y} + z\frac{\partial g}{\partial z} + Ng. \quad (2)$$

Assigning the structural index ($N$) and evaluating the right-hand side and the coefficients on the left-hand side of eq. (2) for at least four points, a system of linear equations can be obtained and solved for the unknown parameters. Within a moving window containing $n \times n$ data points ($n > 2$), it becomes an overdetermined problem that can be solved using the least-squares method to obtain the four unknowns and their uncertainties (standard deviations).

The main difficulty encountered in the application of ED is the choice of the correct structural index, which is critical for meaningful estimation of the depth to the source (Reid 1995; Hus 2002).

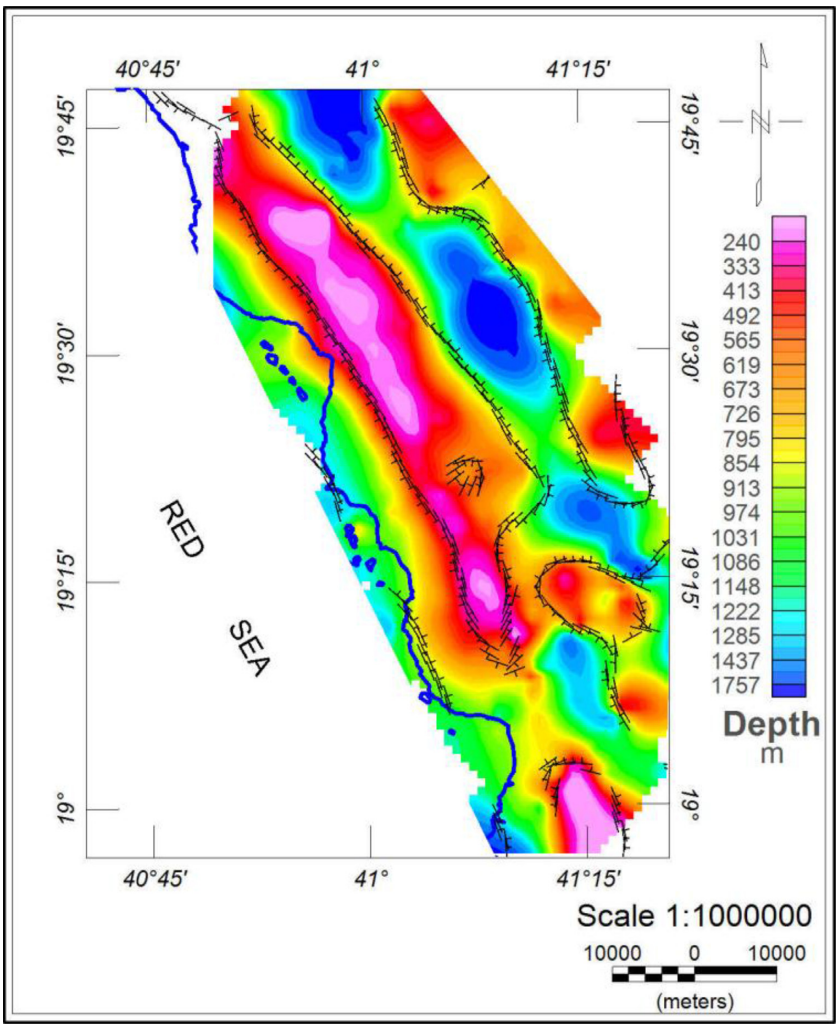


**Figure 13.** The depth-to-basement map based on the modelled profiles in comparison to the block boundaries delineated by SED technique (Fig. 6).

In other words, an inappropriate choice of the structural index can cause serious bias in the depth estimation.

The Euler method was applied to the first vertical derivative of the filtered residual Bouguer anomaly data (Fig. 8). A suitable window size (3000 m) and structure index (SI = 0) were used to map and estimate the depth to fault structures. The method provided basement faults location and reasonable estimations of the depths to these structures, which ranged from 750 to 2250 m. The Euler depth solutions (Fig. 8) also provided support for the idea of tilted fault blocks, and the depth variation matches well with the block boundaries and the vertical movements. The maximum depths were obtained in the northeastern part of the map in coincidence with the basin zone of the down-faulted area.

### 3.5 2-D modelling

The depths and structures obtained from aforementioned techniques were used to set up the starting models for 13 representative gravity profiles (Fig. 9) using the GM-SYS package. Favouring simplicity and to avoid overinterpretation of the data without hard constraints pertaining to basement depth or density of the sedimentary sequence, the basement was modelled with a uniform density of 2.67 g $cm^{-3}$, and the sedimentary section was assumed to have a constant density of 2.3 g $cm^{-3}$. In real world, the density of sediments will tend to increase with depth due to the overburden pressure. Therefore, the estimated thickness of the sedimentary section, assuming constant density, represents a lower limit. The initial models were refined and optimized through iterations of forward modelling, and the inversion was applied as the final optimization until the lowest root-mean-square error was attained. Intersection points of the modelled profiles were considered control points to check the conformity of the final models from line to line.

The modelled sections for three selected profiles are shown in Figs 10–12. The solutions of the ED techniques for the contact model are displayed as red circles over the modelled sections, depicting the obtained locations and depths. The clear match between the Euler solutions and model features strengthens our confidence in the interpreted structures. The first section is for profile L6007, which extends for about 70 km in an NW–SE direction in the northeastern part of the area. The gravity values along this profile range from –20 to 5 mGal. The depth to the basement surface, as shown by the model (Fig. 10), ranges from 200 to 2200 m. This profile cuts across three basement depressions formed by a set of normal faults.

The second profile (6292) extends for about 30 km in an NE–SW direction and has gravity values ranging from –18 to 12 mGal (Fig. 11). The final model shows that the depth to basement ranges from 150 to 1800 m. This model represents well the shape of the tilted fault blocks, with one basin towards the east (the end of the profile) with maximum depth of about 1800 m.

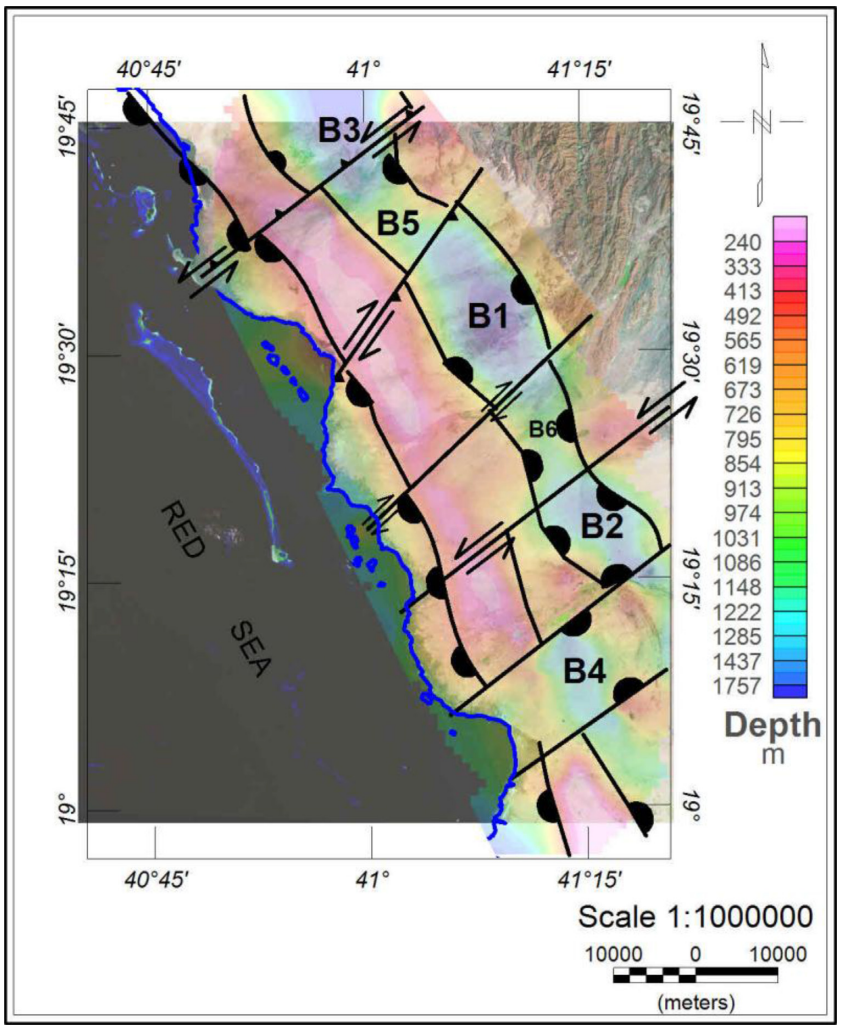


**Figure 14.** Interpreted basement tectonics superimposed on a satellite image and depth map.

The third profile (89) runs in an NE-SW direction with a length of about 35 km and has gravity anomalies ranging from -10 to 10 mGal (Fig. 12). The modelled depth to basement ranges from 200 to 1200 m, showing the southward extension of the tilted fault blocks interpreted from the previous profile (9262), with a basin area towards the east (the end of the profile) with a maximum depth of about 1800 m.

The constructed models depict the variation of basement depth from 0 to 2200 m beneath the ground surface. In general, the depth to basement increases towards the west through local elevations related to the tilted fault-block structure that is dominant in the Red Sea rift zone. The depth to basement obtained along the modelled profiles is gridded and displayed as a basement depth map shown in Fig. 13. This map shows an excellent match between the modelled lines in terms of depth to basement and density contrast. Overlying the depth map, the edges of the causative structures mapped by the SED technique are displayed for comparison. Besides the coincidence of the SED solutions and model structures, SED solutions are located at asymmetric distance, to the east and west, from the peak of the major positive anomaly elongated NNE-SSW. This can be explained by variation of the dip of the block bounding faults, which is high-angle, and low-angle normal faults east and westwards, respectively.

An integration of analysis and interpretation technique results is presented in the interpreted tectonic basement map, summarizing structural setting of the area (Fig. 14). Two fault systems were recognized in the area, a normal fault system trending NNW–SSE that is related to the Red Sea rift and a cross-cutting oblique fault system trending NE–SW. The interaction between these two fault systems resulted in the formation of a set of closed basins elongated in the NNW–SSE direction and terminated by the NE–SW fault system. The geomorphology and sedimentary sections of these basins qualify them as areas of potential groundwater accumulation. Moreover, the cross-cutting NE–SW structures are expected to act as pathways for groundwater discharge to the Red Sea or for seawater invasion into the groundwater.

## 4 CONCLUSIONS

An integrated interpretation of gravity data revealed that the depth to basement (sediment thickness) ranges from a few m to 2200 m. This basement depth variation occurs through local elevations controlled by the tilted fault-block structure dominating the Red Sea rift zone.

The main depressions of the top of basement, situated in the eastern part of the investigated area, are parallel to the Red Sea coast. These depressions are controlled by two fault systems that

affect the area. The first is a normal fault system trending NNW–SSE that is related to the Red Sea rift, and the second is a cross-cutting oblique strike-slip fault system trending NE–SW. These NE-trending faults cut and laterally displace the NNW-trending faults, proving the younger age of movement. The interaction between these two fault systems resulted in the formation of a set of closed basins elongated in the NNW–SSE direction and terminated by the NE–SW fault system. These basins, located west of the Red Sea mountain escarpment, have a thick sedimentary succession and, hence, could be suitable for potential groundwater accumulation. Moreover, the cross-cutting NE–SW structures are expected to act as pathways for groundwater discharge to the Red Sea or seawater invasion into the groundwater.

## ACKNOWLEDGEMENTS

The authors would like to extend their sincere appreciation to the Deanship of Scientific Research at King Saud University for funding this research through the research group no. (RG-1435–029).

## REFERENCES

Bird, D., 1997. Interpreting magnetic data: Geophysical corner, EXPLORER, AAPG, and SEG, May, 1997.

Blakely, R.J. & Simpson, R.W., 1986. Approximating edges of source bodies from magnetic or gravity anomalies, *Geophysics,* **51**(7), 1494–1498.

Gettings, M.E., 1983. A simple Bouguer gravity anomaly map of southwestern Saudi Arabia and an initial interpretation, Open File Rep. USGS-OF-03-94, pp. 89, Saudi Arabia Deputy Ministry for Mineral Resource, (U.S. Geol. Survey, Saudi Arabia Mission), Jeddah.

Healy, J.H., Mooney, W.D., Blank, H.R., Gettings, M.E., Kohler, W.M., Lamson, R.J. & Leone, L., 1982. Saudi Arabian seismic deep-refraction profile, final project report, U.S. Geol. Surv., Saudi Arabian Mission Open-File Rep. 2–37.

Hood, P.J., 1965. Gradient measurements in aeromagnetic surveying, *Geophysics,* **30,** 891–902.

Hus, S., 2002. Imaging magnetic sources using Euler's equation, *Geophys. Prospect.,* **50,** 15–25.

Prinz, C., 1984. Geology map of the Wadi Haliy Quadrangle, sheet 18E, Kingdom of Saudi Arabia, Ministry of Petroleum and Mineral Resources Deputy Ministry for Mineral resources, U.S. Geol. Surv., Saudi Arabia Mission.

Reid, A.B., 1995. Euler deconvolution: Past, present and future-a review, in *SEG Technical Program Expanded Abstracts1995,* pp. 272–273.

Reid, A.B., Allsop, J.M., Granser, H., Millet, A.J. & Somerton, I.W., 1990. Magnetic interpretation in three dimensions using Euler deconvolution, *Geophysics,* **55,** 80–91.

Roy, L., Agarwal, N.P. & Shaw, R.K., 2000. A new concept in Euler deconvolution of isolated gravity anomalies, *Geophys. Prospect.,* **48,** 559–575.

Simpson, R.W., Jachens, R.C. & Blakely, R.J., 1983. AIRYROOT: a FORTRAN program for calculating the gravitational attraction of an Airy isostatic root out to 166.7 km, US Geological Survey Open-File Report, 83, p. 883.

Stavrev, P.Y., 1997. Euler deconvolution using differential similarity transformations of gravity or magnetic anomalies, *Geophys. Prospect.,* **45,** 207–246.

Thompson, D.T., 1982. EULDPH: a new technique for making computer-assisted depth estimates from magnetic data, *Geophysics,* **47,** 31–37.